

New Benchmark of X-ray Line Emission Models of Fe XVII

M. F. Gu

Lawrence Livermore National Laboratory, 7000 East Avenue, Livermore, CA 94550

ABSTRACT

We review the accuracy of existing Fe XVII X-ray line emission models by comparing them with an extensive analysis of *Chandra* high energy transmission grating (HETG) observations of stellar coronae. We find significant discrepancies between most theoretical predictions and observations for at least some of the intensity ratios involving the six principal Fe XVII lines, 3C (15.01 Å), 3D (15.26 Å), 3E (15.45 Å), 3F (16.78 Å), 3G (17.05 Å), and M2 (17.10 Å). We suggest that the main problem of most previous theoretical studies to their inability to fully include electron correlation effects in the atomic structure calculations, while any deficiencies in the scattering approximation methods are of minor importance, regardless of it being close-coupling (CC) or distorted-wave (DW). An approximate method based on the many-body perturbation theory and DW approximation is proposed to include such correlation effects in the calculation of collisional excitation cross sections. The results are shown to agree with coronal observations and laboratory measurements better than most previous theories. Using the new atomic data, we then investigate the electron density sensitivity of the M2/3G intensity ratio and provide an improved density diagnostic tool for astrophysical observations.

Subject headings: atomic data — atomic processes — line: formation — X-rays: general

1. Introduction

There are several widely known problems in the theoretical modeling of Fe XVII X-ray emission lines, making it difficult to use them as reliable diagnostic tools for electron density, temperature, plasma opacity, and iron abundances in X-ray astronomy. The first problem is related to the intensity ratio of the $2p_{3/2}$ - $3d_{5/2}$ transition at 15.26 Å, generally referred to as 3D, to the $2p_{1/2}$ - $3d_{3/2}$ transition, or 3C. Most theoretical predictions of this ratio are smaller than astrophysical observations (Xu et al. 2002; Brinkman et al. 2000;

Canizares et al. 2000; Mewe et al. 2001; Behar et al. 2001) and laboratory measurements (Brown et al. 1998, 2001b; Beiersdorfer et al. 2001). This discrepancy has been used in the past to infer plasma opacity as the stronger 3C line is more susceptible to resonant scattering (Waljeski et al. 1994; Saba et al. 1999). However, this diagnostics depends critically on knowing the optically thin limit of the 3D/3C ratio. The second problem concerns the intensity ratio of the $2p$ - $3s$ (hereafter $3s$) transitions, including 3F (16.78 Å), 3G (17.05 Å), and M2 (17.10 Å), to the $2p$ - $3d$ (hereafter $3d$) transitions, including 3C, 3D, and a much weaker 3E (15.45 Å). The astrophysical observations and laboratory measurements are also significantly larger than most theoretical values (Phillips et al. 1999; Beiersdorfer et al. 2002, 2004) for this ratio. Finally, the theoretical predictions of the intensity ratio of the two $2p$ - $3s$ transitions, M2 to 3G, have also been shown to be significantly smaller than astrophysical observations of low density plasmas (Ness & Schmitt 2005). The M2/3G ratio is density sensitive, and have been used to infer electron densities in magnetic cataclysmic variables (Mauche et al. 2001). However, the inability of reproducing the low density limit of this ratio in theory introduces additional uncertainties in the density determination.

There have been claims that these modeling problems have been solved with large scale close-coupling calculations of the electron collisional excitation data of (Chen & Pradhan 2002; Chen et al. 2003). The new theoretical values of certain line ratios have been shown to agree with laboratory measurements and a few astrophysical observations to within 10%. However, the cross section measurements of the 3C and 3D lines (Brown et al. 2006) indicate that such apparent agreements are rather fortuitous. The more recent work of Chen (2007) and Chen (2008b) revised their earlier work by including pseudo states and the $3d^2$ pair excitation configuration in the target wavefunction expansion and obtained 15-20% reductions in the 3C cross sections compared with Chen et al. (2003), while those of 3D changed little. Chen (2008a) further suggested that the theoretical radiative recombination (RR) cross sections into the M-shell of Fe XVI used for normalization in Brown et al. (2006) are underestimated by 25%, leading to smaller measured 3C and 3D cross sections. In this paper, we provide a thorough assessment of the accuracies of existing atomic calculations on Fe XVII by comparing them with a large sample of *Chandra* observations of stellar coronae obtained with the high energy transmission grating (HETG) spectrometer. We conclude that most of the existing predictions do not offer satisfactory explanation of the observed line ratios. The recent calculations of Chen (2007) and Chen (2008b) provide the best agreement with the laboratory 3C and 3D cross sections. However, a detailed comparison of these data with the *Chandra* observations cannot be done, as the full results of the calculations including all levels necessary for collisional radiative modeling are not available. The major drawback of Chen (2007) and Chen (2008b) is that it is not clear that the accounting the target correlation effects has fully converged. In these calculations, the largest improvement comes

with the inclusion of $3d^2$ pair excitation configuration. However, it is well known that such pair correlations are notoriously slowly convergent. In this paper, we propose a many-body perturbation correction procedure for the excitation cross section calculations, taking all singly and doubly excited correlations into account, but treating their effects on excitation cross sections approximately. We show that the results agree well with Chen (2007) and Chen (2008a) for the 3C and 3D cross sections, and all Fe XVII line ratios are brought into agreement with the *Chandra* observations.

2. Review of existing theoretical calculations

Theoretical study of Fe XVII X-ray lines and their applications in astronomy have a long history. Bely & Bely (1967) obtained the excitation cross sections of $2p^53l$ configurations using the Coulomb-Born approximation. Louergue & Nussbaumer (1973, 1975) developed collisional radiative models of Fe XVII and Ni XIX with DW collision strengths, and compared the resulting line intensities with solar observations. Smith et al. (1985), Raymond & Smith (1986), and Goldstein et al. (1989) pointed out the importance of resonant excitation and its role in determining the temperature dependence of Fe XVII line ratios. Bhatia & Doschek (1992) presented a complete set of Fe XVII line intensities obtained with the DW approximation. Cornille et al. (1994) studied the Fe XVI satellite transitions that blend with Fe XVII lines. Mohan et al. (1997) investigated the effects of relativistic term coupling effects of the Fe XVII collision strengths using the Breit-Pauli R -matrix approximation.

Beiersdorfer & Wargelin (1994) built a flat crystal spectrometer on the electron beam ion trap (EBIT) of the Lawrence Livermore National Laboratory (LLNL), and conducted the first laboratory measurement of Fe XVII X-ray line emission. Brown et al. (1998) carried out a systematic investigation of the Fe XVII lines with the same spectrometer and EBIT facility, and showed that most previous theories significantly underestimate the 3D/3C ratio. Beiersdorfer et al. (2002, 2004) showed that the $3s/3d$ ratio is also underestimated in theory by large factors as compared with both EBIT and Tokamak measurements. Independent laboratory measurements by Laming et al. (2000) with the National Institute of Technology and Standards (NIST) EBIT obtained 3D/3C ratios that are consistent with those from the LLNL EBIT, but reported $3s/3d$ ratios very different from those measured at the LLNL EBIT and concluded that the $3s/3d$ ratios are consistent with modern theoretical calculations. These laboratory work prompted new theoretical studies to resolve these discrepancies. Bhatia & Doschek (2003) improved the earlier work of Bhatia & Doschek (1992) by including more configurations and computing collision strengths in a wider energy range. Doron & Behar (2002) investigated the effects of resonant excitation, recombination

of Fe XVIII and inner-shell ionization of Fe XVI as line formation processes using the Hebrew University Lawrence Livermore Atomic Code (HULLAC), and concluded that such a multi-ion approach increases the $3s/3d$ ratios, bringing them in better agreements with laboratory measurements and astrophysical observations. Gu (2003) reached similar conclusions and also showed that recombination processes are important for other iron ions. Chen & Pradhan (2002), Chen et al. (2003) and Chen & Pradhan (2005) carried out a large scale Breit-Pauli R -matrix calculation for electron collisional excitation of Fe XVII, and claimed that their results resolve the discrepancies between theories, laboratory measurements, and astrophysical observations. An independent close-coupling calculation with the Dirac atomic R -matrix code (Loch et al. 2006) confirms some of the findings in Chen et al. (2003), but found remaining discrepancies between theories and measurements. Most recently, Chen (2007) and Chen (2008b) revised their earlier work by including pseudo states and the $3d^2$ pair excitation configuration in the target wavefunction expansion, and obtained significantly lower $3C$ cross sections than Chen et al. (2003).

In the present paper, we concentrate on these newer theoretical work. A comparison of the Fe XVII line ratios from these calculations are shown in Figure 1, along with the predictions from the widely used astrophysical plasma emission code (APEC) of Smith et al. (2001), which is based on DW collisional data without resonances. All line ratios involved are calculated at the low electron density limit of $\leq 10^{10} \text{ cm}^{-3}$. It is immediately clear from this comparison that the predictions from APEC and Bhatia & Doschek (2003) are very different from those of Doron & Behar (2002), Gu (2003), and Loch et al. (2006). These differences can be attributed to the lack of resonant excitation contributions in APEC and Bhatia & Doschek (2003). On the other hand, the results of Doron & Behar (2002) and Gu (2003) are relatively close to each other both in the temperature dependence of the line ratios and their magnitudes, which is not surprising since the two calculations employ essentially the same physics and approximations. The relatively large difference in the $3E/3C$ ratio between Doron & Behar (2002) and Gu (2003) can be attributed to the incomplete treatment of resonant excitation in Doron & Behar (2002). The results of Gu (2003) and Loch et al. (2006) are also in very good agreement, although Loch et al. (2006) generally produce a steeper temperature dependence of the line ratios, especially for the $3s/3d$ ratios. This is due to the fact that Loch et al. (2006) do not include recombination contributions to the line intensities. Recombination preferentially enhances the $3s$ transitions and has larger contributions at higher temperatures due to the higher fractional abundance of Fe XVIII relative to Fe XVII. One surprising fact in this comparison is the relatively large differences between the $3F/3C$ ratios of Chen et al. (2003), $3s/3d$ ratios of Chen & Pradhan (2005), and the corresponding ratios of Loch et al. (2006). In fact, the ratios of Chen et al. (2003) and Chen & Pradhan (2005), which include resonant excitation, are similar to the DW values

without resonant excitation. Loch et al. (2006) showed that the differences in the 3C and 3D cross sections in the two R -matrix calculations are small. Therefore the large differences we note in this comparison are due to the differences in the $3s$ intensities. The updated 3C and 3D cross sections of Chen (2007) give larger 3D/3C ratios than all other calculations. Because the full results of the new calculations of Chen (2007) are not available, we scaled the 3F/3C and $3s/3d$ ratios of Chen et al. (2003) and Chen & Pradhan (2005) to reflect the updated 3C and 3D cross sections, but keeping $3s$ intensities unchanged. These scaled ratios for 3F/3C become close to those of Gu (2003) and Loch et al. (2006), but those for $3s/3d$ are still significantly smaller.

3. *Chandra* stellar observations of Fe XVII spectra

In order to assess the accuracies of various calculations, we compare them with an extensive set of stellar coronal observations with the HETG spectrometer aboard *Chandra* X-ray observatory. Since its launch, *Chandra* has observed a large sample of stellar coronal sources with the high resolution HETG spectrometer. Table 1 lists the sources in our selection. The data were retrieved from the *Chandra* archive, and reprocessed with CIAO version 3.4 and CALDB version 3.4. Some sources are observed multiple times, and we combine the individual observations to improve the statistics. There are 11 sources that do not provide decent counting statistics individually, and we have also combined them to produce a single composite observation referred to as “Stack” in Table 1. Of the 24 targets (after grouping of multiple observations and weak sources) in our sample, Capella provides the best statistical quality because it is an calibration target, and observed many times.

We follow the differential emission measure (DEM) analysis method of Gu et al. (2006) to characterize the coronal property of these sources. Using the APEC database modified by the line emissivities of Gu (2003) and wavelengths of Gu (2005), we reconstruct the DEM distribution and elemental abundances of the coronal plasma by jointly fitting the ± 1 orders of medium and high energy grating (MEG and HEG) spectra. The resulting DEM and comparison of theoretical and observed spectra in the 12–18 Å region is shown in Figures 2 and 3 for the composite observation of Capella. The DEM is peaked near $10^{6.9}$ K, which is similar to the result of Gu et al. (2006) using a single observation. To characterize the temperature of the Fe XVII emission regions, it is more appropriate to examine the DEM weighted by the Fe XVII emissivities, which is also shown in Figure 2. It indicates that the Fe XVII emissivity weighted DEM has a narrower profile. In fact, the characteristic temperatures of the Fe XVII emission regions are always in the range of $10^{6.6}$ – $10^{6.9}$ K for all sources, even though some of them have significant high temperature tails beyond 10^7 K.

This is due to the fact that Fe XVII fractional abundance peaks near $10^{6.6}$ K in collisional ionization equilibrium.

The spectral model shown in Figure 3 already provides a reasonable fit to the observed spectrum. However, close inspection of the Fe XVII lines reveal significant discrepancies between them. Using the reconstructed spectrum as a basis, we obtain a better fit to the Fe XVII emission by varying 3C, 3D, 3E, 3G, 3F, and M2 line intensities. Brown et al. (2001a) and Brickhouse & Schmelz (2006) demonstrated that the 3D line blends perfectly with an Fe XVI satellite transition, and another nearby Fe XVI transition at 15.21 Å can be used to remove the Fe XVI contribution to the 3D line. Many of the sources in our sample indicate the presence of the 15.21 Å line, providing a measure of contamination to the 3D line. The 15.21 Å line intensity is extracted from the measured spectra and multiplied by a factor of 0.7, which is then subtracted from the apparent 3D intensity. The branching ratio of 0.7 used here is determined with the Flexible Atomic Code developed by the author, and is between the values 0.83 used by Brickhouse & Schmelz (2006) and 0.51 used by Brown et al. (2001a). However, because the Fe XVI contamination of the 3D line is relatively small, the correction decreases the measured 3D/3C ratio only by $\sim 10\%$. The differences in the branching ratios leads to 2–3 % differences in the 3D/3C ratio, which are smaller than the statistical errors for most sources. The derived line ratios for the 24 sources are listed in Table 2. The Fe XVII emissivity weighted average temperature, T_{em} , of the coronae are also shown. Ness et al. (2003) reported the ratios involving the 3C, 3D and 3F lines for a large sample of coronal sources observed by *Chandra* and *XMM-Newton*. The results obtained here are generally consistent with those of Ness et al. (2003) for the set of common sources.

In comparing the measured and theoretical line ratios, the calculations should ideally be performed for the appropriate DEM distributions. In practice, we find that the ratios calculated with the DEM is very close to the ones calculated at a single temperature of T_{em} . This is demonstrated in Figure 4 for the 8 line ratios we investigate. In the rest of the paper, we therefore use the isothermal line ratios calculated at T_{em} for comparison.

Figure 5 shows the comparison of measured and theoretical line ratios in detail. Because the predictions of Doron & Behar (2002) are generally similar to those of Gu (2003), and those of Bhatia & Doschek (2003) are similar to those of APEC, we omit those from Figure 5 to reduce clutter. It is clear that none of the theories can explain all line ratios satisfactorily. All theoretical ratios are below the measured ones, except for 3D/3C, where the results of Chen (2007) agree with the measurements, 3E/3C and 3F/3C, where the values of Loch et al. (2006), Gu (2003), and the results of Chen et al. (2003) scaled for the new 3C cross sections of Chen (2007) agree with the measurements, and M2/3G, where the values of APEC agree with the measurements. However, it should be pointed out that the measured

3E/3C ratio have large statistical uncertainties. The APEC ratios of M2/3C and 3G/3C are very different from the measurements, and the agreement for M2/3G is therefore fortuitous. Despite the claim of excellent agreements between their theoretical line ratios, laboratory measurements and astrophysical observations in Chen & Pradhan (2002), Chen et al. (2003), and Chen & Pradhan (2005), we find their theoretical values are significantly smaller than the *Chandra* measurements for the 3F/3C and 3s/3d ratios, even more so than the calculations of Loch et al. (2006) and Gu (2003). After scaling for the new lower 3C cross sections of Chen (2007), the 3s/3d ratios are still smaller than the *Chandra* observations. Since the data from Chen et al. (2003) and subsequent work are not publicly available, we are not able to calculate other line ratios for thermal plasmas for a more detailed comparison.

4. Distorted-wave with many-body perturbation correction

The fact that the calculations of Gu (2003) and Loch et al. (2006) agree with each other very well except for the differences in the recombination contributions indicates that the two theoretical methods, DW in Gu (2003) and *R*-matrix in Loch et al. (2006) are of comparable quality for Fe XVII. The differences between measured and calculated line ratios are not due to deficiencies in the scattering approximations. The cross section measurements for 3C and 3D lines of Brown et al. (2006) demonstrated that theories tend to overestimate the 3C cross sections more than 3D. The general trend in the comparison of theories and *Chandra* measurements indeed support this picture. If the theoretical 3C cross sections were to decrease by $\sim 20\%$, the predictions of Gu (2003) and Loch et al. (2006) would agree with the observations much better. 3C is a dipole allowed transition, its collisional excitation cross section is nearly proportional to the oscillator strength, which is determined solely by atomic structure calculations. Therefore we suspect that the root problem in the previous theories of Fe XVII line intensities is the incomplete treatment of electron correlation effects in the target ion. This conclusion is supported by the comparison of various oscillator strengths calculations for 3C and 3D listed in Table 2 of Chen et al. (2003). Of these calculations, the many-body perturbation theory (MBPT) treatment of Safronova et al. (2001) is likely to be the most accurate in describing electron correlation effects in Fe XVII, which also yields the smallest oscillator strength for the 3C transition. The recent calculations of Chen (2007) and Chen (2008b) also showed that by improving the target wavefunction expansion, the 3C cross sections are reduced by 15-20%. However, it is not clear that the target description in Chen (2007) and Chen (2008b) has fully converged, given that the largest change comes with the inclusion of the $3d^2$ pair excited configuration, and such pair correlations are known to be notoriously slowly convergent.

We have developed an independent MBPT method within the framework of FAC for general open-shell ions, and have used it in calculating the wavelengths of iron and nickel L-shell X-ray transitions (Gu 2005). We recently extended the method to also calculate radiative transition rates and oscillator strengths. The 3C and 3D weighted oscillator strengths calculated in our MBPT method are 2.17 and 0.62, respectively. This compares to 2.50 and 0.62 calculated by the DW approximation. These independent MBPT calculations therefore suggest that the 3C cross sections are likely to be overestimated by as much as $\sim 10\text{--}20\%$ in previous non-MBPT calculations. Chen (2007) gave the weighted oscillator strengths of 3C and 3D to be 2.25 and 0.635, respectively, which agree with our MBPT results very well. This indicates the near convergence of their accounting of Fe XVII target correlation effects.

However, the extension of the MBPT method to treat collisional excitation processes is rather difficult beyond the plane-wave Born approximation. Here we propose an approximate procedure for including MBPT corrections in the calculation of DW excitation cross sections. Bar-Shalom et al. (1988) showed that the DW collision strengths can be factorized to contain angular and radial integrals as follows

$$\Omega_{01} = 2 \sum_k \sum_{\substack{\alpha_0 \alpha_1 \\ \beta_0 \beta_1}} Q^k(\alpha_0 \alpha_1; \beta_0 \beta_1) \langle \psi_0 || Z^k(\alpha_0, \alpha_1) || \psi_1 \rangle \langle \psi_0 || Z^k(\beta_0, \beta_1) || \psi_1 \rangle, \quad (1)$$

where α, β denote bound orbitals making the transition, Z^k are angular factors, and Q^k are radial integrals involving partial-wave sum

$$Q^k(\alpha_0 \alpha_1; \beta_0 \beta_1) = \sum_{\kappa_0 \kappa_1} [k]^{-1} P^k(\kappa_0 \kappa_1; \alpha_0 \alpha_1) P^k(\kappa_0 \kappa_1; \beta_0 \beta_1), \quad (2)$$

and

$$P^k(\kappa_0 \kappa_1; \alpha_0 \alpha_1) = X^k(\alpha_0 \kappa_0; \alpha_1 \kappa_1) + \sum_t (-1)^{k+t} [k] \begin{Bmatrix} j_{\alpha_0} & j_1 & t \\ j_0 & j_{\alpha_1} & k \end{Bmatrix} X^t(\alpha_0 \kappa_0; \kappa_1 \alpha_1), \quad (3)$$

where κ represents a continuum orbital and X^k are the usual Slater integrals. The first term in P^k is the direct contribution, and the second term is the exchange contribution. In the Coulomb-Bethe approximation, the direct term can be written as

$$P_{CB}^k(\kappa_0 \kappa_1; \alpha_0 \alpha_1) = M_k(\alpha_0 \alpha_1) R_k(\kappa_0 \kappa_1), \quad (4)$$

where

$$\begin{aligned} M_k(\alpha_0 \alpha_1) &= \langle \alpha_0 || C^k || \alpha_1 \rangle \int (P_{\alpha_0} P_{\alpha_1} + Q_{\alpha_0} Q_{\alpha_1}) r^k dr \\ R_k(\kappa_0 \kappa_1) &= \int (P_{\kappa_0} P_{\kappa_1} + Q_{\kappa_0} Q_{\kappa_1}) \frac{1}{r^{k+1}} dr, \end{aligned} \quad (5)$$

where C^k is the normalized spherical harmonic, P_α and Q_α are the large and small components of the Dirac radial wavefunctions of orbital α . Note that M_k depends only on the target orbitals and is proportional to the electric multipole integral of rank k . This integral is the same as the one used in radiative transition rate calculations. Therefore, the ratio of the MBPT corrected to the conventional DW direct excitation contributions is the same as the ratio of the MBPT corrected to uncorrected oscillator strengths. We calculate such ratios from the radiative transition rates with and without MBPT effects, and use them as scaling factors to correct the direct excitation contributions to P^k , and obtain the MBPT corrected collision strengths in the DW approximation.

Following the procedure outlined above, and the three-ion model of Gu (2003), we recalculate the Fe XVII line ratios and compare them with the *Chandra* observations in Figure 6. The results of Loch et al. (2006) are shown again for easy comparison. It is obvious that our MBPT corrections bring the calculated line ratios into much better agreement with *Chandra* observations. The M2/3C and M2/3G ratios seem to be still slightly below the observed ones, but show significant improvements over the existing theories.

Finally, we compare the MBPT corrected effective formation cross sections of the 3C and 3D transitions with laboratory measurements of Brown et al. (2006) in Figure 7. Our effective cross sections include contributions of resonant excitation and radiative cascades from higher levels. The cross sections of Gu (2003), Chen et al. (2003), Loch et al. (2006), and Chen (2007) are also shown for comparison. The *R*-matrix calculations include resonances, but do not taken into account radiative cascades. Clearly, the MBPT corrections leave the 3D cross sections of Gu (2003) almost unchanged, but decrease the 3C cross sections by about 18%. The cross sections of Chen et al. (2003) and Loch et al. (2006) are all higher than the present MBPT corrected values for 3C. The cross sections of Chen (2007) are only slightly lower than the present calculations by $\sim 5\%$, which likely represents the differences between different scattering approximations. However, the present MBPT corrected cross sections for both 3C and 3D are still about 15% higher than the laboratory measurements overall, while the 3D/3C ratios agree with each other very well. The energy dependence of the measured cross sections shown in Figure 7 were obtained by sweeping the electron beam energies and recording the energy dependence of the 3C and 3D line intensities. They are normalized to the RR emission into the M-shell of Fe XVI at a single energy point of 964 eV. There is significant statistical fluctuation in the measured data, but the overall discrepancies between the measured values and the present calculations are less than 15%, especially at the near threshold region below 1200 eV. The discrepancies between the measured values and the results of Chen (2007) are even smaller, at 10% level. If the suggestion that the RR cross sections used in Brown et al. (2006) are underestimated by 25% (Chen 2008a) is correct, the new theoretical cross sections of 3C and 3D of the present paper and those of Chen (2007)

and Chen (2008b) would have become smaller than the renormalized measurements.

Since our new Fe XVII line ratios agree with *Chandra* observations, the lower experimental 3C and 3D cross sections would lead to lower cross sections for all other lines as well, and to inaccurate iron abundance determinations if these lines are used as main constraints. The cross sections of Brown et al. (2006) were determined by normalizing the collisional excitation lines to the RR emission onto the M-shell of Fe XVI. The overall normalization uncertainties were estimated to be on the order of 10%. The differences between our new calculations and the measurements are therefore not significantly larger than the experimental uncertainties, especially if one takes into account that the more elaborate R-Matrix scattering method seems to further lower the cross sections by $\sim 5\%$.

5. Density diagnostics with the M2 line

Due to the relatively slow radiative decay of the M2 transition, the M2 line is collisionally quenched at electron densities above 10^{13} cm^{-3} . The M2/3G ratio has been used to infer electron densities in magnetic cataclysmic variables (Mauche et al. 2001) and stellar coronal sources (Ness & Schmitt 2005). However, §3 shows that the M2/3G ratios of all coronal sources with densities known to be below 10^{12} cm^{-3} are significantly larger than previous theoretical predictions, which is identified as a major problem in applying this diagnostic in Ness & Schmitt (2005). We note that Ness & Schmitt (2005) seem to indicate that the low density limit of M2/3G calculated with Gu (2003) data agree with the coronal observations. We have since confirmed that it is due to some misinterpretation of the Gu (2003) data in calculating the M2/3G ratio, and the Gu (2003) ratio of M2/3G is in fact much lower than the observations. The present MBPT corrected M2/3G ratio, although appears to be still slightly lower overall, is at least marginally consistent with low density coronal observations.

In Figure 8, we show the density dependence of the emissivities of the six Fe XVII lines at a temperature of $10^{6.7} \text{ K}$ in comparison with the predictions of Loch et al. (2006). The publicly released data from Loch et al. (2006) do not include forbidden transition rates. In order to derive the density dependence of line emissivities, we augmented their dataset with the forbidden transition rates from the present calculations. Two major differences are seen between the present work and that of Loch et al. (2006), namely, the smaller 3C (due to MBPT correction) and larger M2 (due to recombination contributions) in the present calculation, which helps to explain the observed coronal values. The density dependence of M2/3G ratios in the present calculation and those of Loch et al. (2006) are shown in Figure 9 for two electron temperatures, $10^{6.7}$ and $10^{7.2} \text{ K}$. The differences between the present work and Loch et al. (2006) are even more pronounced at higher temperatures due to the

increasing importance of recombination contributions to the M2 line intensity.

6. conclusions

We have conducted a systematic study of the Fe XVII emission lines of stellar coronal sources observed by the HETG spectrometer aboard *Chandra*. At least some of the line ratios involving the six principal Fe XVII lines are shown to disagree with most existing theories. The calculations of Doron & Behar (2002) and Gu (2003), which include resonant excitation and recombination contributions in DW approximation provide as good agreement with data as the more sophisticated close-coupling calculation of Loch et al. (2006) with the Dirac atomic *R*-matrix code. Similarly sophisticated, Breit-Pauli *R*-matrix results of Chen & Pradhan (2002); Chen et al. (2003); Chen & Pradhan (2005), however, show worse agreements with the *Chandra* observations for the 3F/3C and 3s/3d line ratios. The source of discrepancies in the two *R*-matrix calculations are not clear. The most recent Breit-Pauli *R*-matrix results of Chen (2007) gave the best agreement with laboratory measurements of 3C and 3D cross sections, but a systematic comparison with *Chandra* line ratios cannot be carried out, as the full results of these calculations necessary for collisional radiative modeling are not available. If we assume that the 3s line intensities of Chen (2007) are the same as Chen et al. (2003) and Chen & Pradhan (2005), and only correct the ratios for the updated 3C and 3D cross sections, the resulting 3D/3C and 3F/3C ratios are in agreement with the *Chandra* observations, but the 3s/3d ratios are still significantly lower than observed values.

Based on the MBPT calculations of oscillator strengths, we suggest that the incomplete treatment of electron correlation effects of the Fe XVII target is the cause of overestimating the 3C cross sections in most previous theories, as is also suggested by the recent calculations of Chen (2007) and Chen (2008b). We propose a simple, MBPT based procedure to incorporate such correlation effects in the calculation of electron collisional excitation cross sections under DW approximation. The resulting Fe XVII line ratios are shown to agree with *Chandra* observations much better than previous predictions. The 3C and 3D cross sections of the present work are only $\sim 5\%$ larger than the calculations of Chen (2007). Comparison of our MBPT corrected 3C and 3D cross sections and the measurements of Brown et al. (2006) suggests remaining discrepancies on the order of 15%, although systematic uncertainties of about 10% may explain part of this difference, and the simplified scattering approximation used here may be responsible for the remaining discrepancies. We have shown that if the RR cross sections used for normalization in Brown et al. (2006) are underestimated by 25%, as suggested by Chen (2008a), the new theoretical cross sections of the present work and those of Chen (2007) and Chen (2008b) would have become smaller than the renormalized

measurements.

We have presented the density dependence of the Fe XVII emissivities and M2/3G ratio, and compared them with previous calculations. The improved low density limit of M2/3G ratio provides greater confidence in applying this density diagnostics in astrophysical observations.

The author would like to thank P. Beiersdorfer for extensive comments on the original manuscript. Support for this work was provided by the National Aeronautics and Space Administration through Chandra Award Number TM7-8001Z issued by the Chandra X-ray Observatory Center, which is operated by the Smithsonian Astrophysical Observatory for and on behalf of the National Aeronautics Space Administration under contract NAS8-03060. This work was performed under the auspices of the U.S. Department of Energy by Lawrence Livermore National Laboratory under Contract DE-AC52-07NA27344.

REFERENCES

- Bar-Shalom, A., Klapisch, M., & Oreg, J. 1988, *Phys. Rev. A*, 38, 1773
- Behar, E., Cottam, J., & Kahn, S. M. 2001, *ApJ*, 548, 966
- Beiersdorfer, P., Behar, E., Boyce, K. R., Brown, G. V., Chen, H., Gendreau, K. C., Gu, M.-F., Gygax, J., Kahn, S. M., Kelley, R. L., Porter, F. S., Stahle, C. K., & Szymkowiak, A. E. 2002, *ApJ*, 576, L169
- Beiersdorfer, P., Bitter, M., von Goeler, S., & Hill, K. W. 2004, *ApJ*, 610, 616
- Beiersdorfer, P., von Goeler, S., Bitter, M., & Thorn, D. B. 2001, *Phys. Rev. A*, 64, 032705
- Beiersdorfer, P. & Wargelin, B. J. 1994, *Review of Scientific Instruments*, 65, 13
- Bely, O. & Bely, F. 1967, *Sol. Phys.*, 2, 285
- Bhatia, A. K. & Doschek, G. A. 1992, *Atomic Data and Nuclear Data Tables*, 52, 1
- . 2003, *Atomic Data and Nuclear Data Tables*, 85, 1
- Brickhouse, N. S. & Schmelz, J. T. 2006, *ApJ*, 636, L53
- Brinkman, A. C., Gunsing, C. J. T., Kaastra, J. S., van der Meer, R. L. J., Mewe, R., Paerels, F., Raassen, A. J. J., van Rooijen, J. J., Bräuninger, H., Burkert, W., Burwitz, V.,

- Hartner, G., Predehl, P., Ness, J.-U., Schmitt, J. H. M. M., Drake, J. J., Johnson, O., Juda, M., Kashyap, V., Murray, S. S., Pease, D., Ratzlaff, P., & Wargelin, B. J. 2000, *ApJ*, 530, L111
- Brown, G. V., Beiersdorfer, P., Chen, H., Chen, M. H., & Reed, K. J. 2001a, *ApJ*, 557, L75
- Brown, G. V., Beiersdorfer, P., Chen, H., Scofield, J. H., Boyce, K. R., Kelley, R. L., Kilbourne, C. A., Porter, F. S., Gu, M. F., Kahn, S. M., & Szymkowiak, A. E. 2006, *Physical Review Letters*, 96, 253201
- Brown, G. V., Beiersdorfer, P., Liedahl, D. A., Widmann, K., & Kahn, S. M. 1998, *ApJ*, 502, 1015
- Brown, G. V., Beiersdorfer, P., & Widmann, K. 2001b, *Phys. Rev. A*, 63, 032719
- Canizares, C. R., Huenemoerder, D. P., Davis, D. S., Dewey, D., Flanagan, K. A., Houck, J., Markert, T. H., Marshall, H. L., Schattenburg, M. L., Schulz, N. S., Wise, M., Drake, J. J., & Brickhouse, N. S. 2000, *ApJ*, 539, L41
- Chen, G.-X. 2007, *Phys. Rev. A*, 76, 062708
- . 2008a, *Phys. Rev. A*, 77, 022703
- . 2008b, *Phys. Rev. A*, 77, 022701
- Chen, G. X. & Pradhan, A. K. 2002, *Physical Review Letters*, 89, 013202
- Chen, G.-X. & Pradhan, A. K. 2005, *ArXiv Astrophysics e-prints*
- Chen, G.-X., Pradhan, A. K., & Eissner, W. 2003, *Journal of Physics B Atomic Molecular Physics*, 36, 453
- Cornille, M., Dubau, J., Faucher, P., Bely-Dubau, F., & Blancard, C. 1994, *A&AS*, 105, 77
- Doron, R. & Behar, E. 2002, *ApJ*, 574, 518
- Goldstein, W. H., Osterheld, A., Oreg, J., & Bar-Shalom, A. 1989, *ApJ*, 344, L37
- Gu, M. F. 2003, *ApJ*, 582, 1241
- . 2005, *ApJS*, 156, 105
- Gu, M. F., Gupta, R., Peterson, J. R., Sako, M., & Kahn, S. M. 2006, *ApJ*, 649, 979

- Laming, J. M., Kink, I., Takacs, E., Porto, J. V., Gillaspy, J. D., Silver, E. H., Schnopper, H. W., Bandler, S. R., Brickhouse, N. S., Murray, S. S., Barbera, M., Bhatia, A. K., Doschek, G. A., Madden, N., Landis, D., Beeman, J., & Haller, E. E. 2000, *ApJ*, 545, L161
- Loch, S. D., Pindzola, M. S., Ballance, C. P., & Griffin, D. C. 2006, *Journal of Physics B Atomic Molecular Physics*, 39, 85
- Loulergue, M. & Nussbaumer, H. 1973, *A&A*, 24, 209
- . 1975, *A&A*, 45, 125
- Mauche, C. W., Liedahl, D. A., & Fournier, K. B. 2001, *ApJ*, 560, 992
- Mewe, R., Raassen, A. J. J., Drake, J. J., Kaastra, J. S., van der Meer, R. L. J., & Porquet, D. 2001, *A&A*, 368, 888
- Mohan, M., Sharma, R., & Eissner, W. 1997, *ApJS*, 108, 389
- Ness, J.-U. & Schmitt, J. H. M. M. 2005, *A&A*, 444, L41
- Ness, J.-U., Schmitt, J. H. M. M., Audard, M., Güdel, M., & Mewe, R. 2003, *A&A*, 407, 347
- Phillips, K. J. H., Mewe, R., Harra-Murnion, L. K., Kaastra, J. S., Beiersdorfer, P., Brown, G. V., & Liedahl, D. A. 1999, *A&AS*, 138, 381
- Raymond, J. C. & Smith, B. W. 1986, *ApJ*, 306, 762
- Saba, J. L. R., Schmelz, J. T., Bhatia, A. K., & Strong, K. T. 1999, *ApJ*, 510, 1064
- Safronova, U. I., Namba, C., Murakami, I., Johnson, W. R., & Safronova, M. S. 2001, *Phys. Rev. A*, 64, 012507
- Smith, B. W., Mann, J. B., Cowan, R. D., & Raymond, J. C. 1985, *ApJ*, 298, 898
- Smith, R. K., Brickhouse, N. S., Liedahl, D. A., & Raymond, J. C. 2001, *ApJ*, 556, L91
- Waljeski, K., Moses, D., Dere, K. P., Saba, J. L. R., Strong, K. T., Webb, D. F., & Zarro, D. M. 1994, *ApJ*, 429, 909
- Xu, H., Kahn, S. M., Peterson, J. R., Behar, E., Paerels, F. B. S., Mushotzky, R. F., Jernigan, J. G., Brinkman, A. C., & Makishima, K. 2002, *ApJ*, 579, 600

Table 1. *Chandra* HETG observations selected in the present sample. Targets with multiple exposures are combined to form a single observation. 11 weak sources are also grouped to form a composite observation for target 15, or “Stack”.

Index	Target	ObsId	Exposure (ks)
1	ξ Uma	1894	70.9
2	AD Leo	2570	45.2
3	τ Sco	638	59.2
4	EV Lac	1885	100.0
5	CC Eri	4513	89.5
6	HD 45348	636	94.6
7	AU Mic	17	58.8
8	44 Boo	14	59.1
9	VW Cep	3766	116.6
10 ^a	Capella	...	297.9
...	Capella	57	28.8
...	Capella	1099	14.6
...	Capella	1100	14.6
...	Capella	1101	14.6
...	Capella	1103	40.5
...	Capella	1235	14.6
...	Capella	1236	14.6
...	Capella	1237	14.6
...	Capella	1318	26.7
...	Capella	2583	27.6
...	Capella	3674	28.7
...	Capella	5955	28.7
...	Capella	6471	29.6
11	HD 93497	3410	57.0
12	AB Dor	16	52.3
13	TZ Crb	15	83.7
14	V824 Ara	2538	94.2
15 ^b	Stack	...	711.7
...	TY Pyx	601	49.1
...	FK Com	614	41.4
...	HD 68273	629	64.9
...	II Peg	1451	42.7
...	HD 206267	1888	34.1
...	HD 206267	1889	39.5
...	HD 111812	1891	130.2
...	HD 223460	1892	95.7
...	PROXIMA Cen	2388	42.4
...	HIP 92680	3729	73.9
...	V4046 Sgr	5423	97.7
16	ER Vul	1887	112.0
17	HR 1099	62538	94.7
18	β Ceti	974	86.1
19	Algol	604	51.7
20 ^c	AR Lac	...	64.3
...	AR Lac	6	32.1
...	AR Lac	9	32.2

Table 1—Continued

Index	Target	ObsId	Exposure (ks)
21	UX Ari	605	48.5
22 ^d	IM Peg	...	192.1
...	IM Peg	2527	24.6
...	IM Peg	2528	24.8
...	IM Peg	2529	24.8
...	IM Peg	2530	23.9
...	IM Peg	2531	23.9
...	IM Peg	2532	22.5
...	IM Peg	2533	23.7
...	IM Peg	2534	23.9
23 ^e	σ Gem	...	120.8
...	σ Gem	5422	62.8
...	σ Gem	6282	57.9
24	λ And	609	81.9

^aSum of the following 13 observations of Capella.

^bSum of the following 11 observations of different targets.

^cSum of the following 2 observations of AR Lac.

^dSum of the following 8 observations of IM Peg.

^eSum of the following 2 observations of σ Gem.

Table 2. Fe XVII line ratios measured with the *Chandra* HETG observations. T_{em} is the Fe XVII emissivity weighted average temperature of sources in units of 10^6 K. The numbers in parentheses are statistical uncertainties. 3s refers to the sum of 3F, 3G, and M2, and 3d refers to the sum of 3C, 3D, and 3E.

Index	Target	T_{em} (MK)	3D/3C	3E/3C	3F/3C	3G/3C	M2/3C	M2/3G	3s/3C	3s/3d
1	ξ Uma	5.13	0.423(0.024)	0.048(0.009)	0.780(0.041)	0.974(0.048)	0.969(0.048)	0.997(0.063)	2.723(0.098)	1.852(0.062)
2	AD Leo	5.30	0.360(0.048)	0.059(0.018)	0.633(0.070)	0.816(0.089)	0.814(0.082)	1.006(0.132)	2.263(0.168)	1.594(0.111)
3	τ Sco	5.32	0.337(0.034)	0.052(0.016)	0.728(0.060)	0.944(0.070)	0.892(0.075)	0.947(0.081)	2.564(0.163)	1.846(0.107)
4	EV Lac	5.33	0.319(0.035)	0.038(0.013)	0.612(0.051)	0.991(0.077)	0.845(0.072)	0.856(0.082)	2.448(0.145)	1.804(0.101)
5	CC Eri	5.54	0.328(0.037)	0.038(0.014)	0.854(0.080)	0.996(0.084)	1.011(0.088)	1.020(0.098)	2.861(0.192)	2.095(0.126)
6	HD 45348	5.59	0.294(0.038)	0.039(0.013)	0.459(0.054)	0.788(0.076)	0.751(0.071)	0.959(0.107)	1.999(0.140)	1.500(0.108)
7	AU Mic	5.63	0.370(0.049)	0.025(0.014)	0.628(0.077)	0.801(0.074)	1.008(0.096)	1.266(0.142)	2.437(0.183)	1.748(0.124)
8	44 Boo	5.72	0.317(0.030)	0.038(0.015)	0.651(0.049)	0.916(0.064)	0.786(0.050)	0.861(0.064)	2.354(0.124)	1.737(0.084)
9	VW Cep	5.72	0.409(0.047)	0.056(0.020)	0.649(0.067)	0.927(0.103)	0.930(0.099)	1.013(0.135)	2.507(0.192)	1.711(0.115)
10	Capella	5.85	0.364(0.004)	0.056(0.002)	0.701(0.005)	0.963(0.005)	0.896(0.005)	0.930(0.000)	2.560(0.015)	1.802(0.009)
11	HD 93497	5.98	0.292(0.026)	0.086(0.015)	0.677(0.051)	1.002(0.066)	0.872(0.067)	0.872(0.066)	2.551(0.147)	1.850(0.093)
12	AB Dor	5.99	0.405(0.040)	0.059(0.018)	0.679(0.049)	0.927(0.067)	0.912(0.066)	0.987(0.078)	2.519(0.140)	1.721(0.086)
13	TZ Crb	6.08	0.325(0.014)	0.057(0.007)	0.603(0.021)	0.875(0.029)	0.756(0.026)	0.866(0.035)	2.233(0.056)	1.616(0.036)
14	V824 Ara	6.17	0.332(0.030)	0.056(0.015)	0.615(0.047)	0.948(0.053)	0.910(0.054)	0.962(0.063)	2.473(0.114)	1.782(0.079)
15	Stack	6.19	0.345(0.030)	0.026(0.012)	0.640(0.044)	0.871(0.055)	0.862(0.050)	0.991(0.057)	2.374(0.121)	1.732(0.083)
16	ER Vul	6.28	0.344(0.034)	0.094(0.017)	0.598(0.053)	0.899(0.077)	0.878(0.070)	0.980(0.080)	2.375(0.161)	1.651(0.096)
17	HR 1099	6.35	0.305(0.020)	0.054(0.011)	0.626(0.034)	0.853(0.044)	0.864(0.042)	1.016(0.059)	2.343(0.088)	1.725(0.059)
18	β Ceti	6.42	0.347(0.016)	0.066(0.007)	0.686(0.029)	0.929(0.032)	0.862(0.030)	0.929(0.040)	2.477(0.067)	1.753(0.043)
19	Algol	6.57	0.372(0.035)	0.061(0.017)	0.686(0.049)	0.993(0.067)	0.857(0.057)	0.865(0.065)	2.536(0.129)	1.771(0.083)
20	AR Lac	6.57	0.400(0.042)	0.014(0.011)	0.640(0.053)	1.017(0.070)	0.907(0.066)	0.895(0.075)	2.564(0.147)	1.814(0.098)
21	UX Ari	6.63	0.314(0.050)	0.027(0.019)	0.601(0.080)	0.631(0.088)	0.740(0.091)	1.187(0.182)	1.971(0.196)	1.471(0.137)
22	IM Peg	6.88	0.327(0.043)	0.085(0.024)	0.610(0.063)	0.766(0.078)	0.832(0.077)	1.094(0.121)	2.209(0.168)	1.565(0.109)
23	σ Gem	6.95	0.322(0.021)	0.053(0.012)	0.603(0.032)	0.851(0.047)	0.883(0.047)	1.040(0.065)	2.337(0.092)	1.700(0.069)
24	λ And	7.02	0.381(0.037)	0.059(0.019)	0.591(0.046)	0.868(0.053)	0.793(0.057)	0.916(0.073)	2.252(0.111)	1.564(0.073)

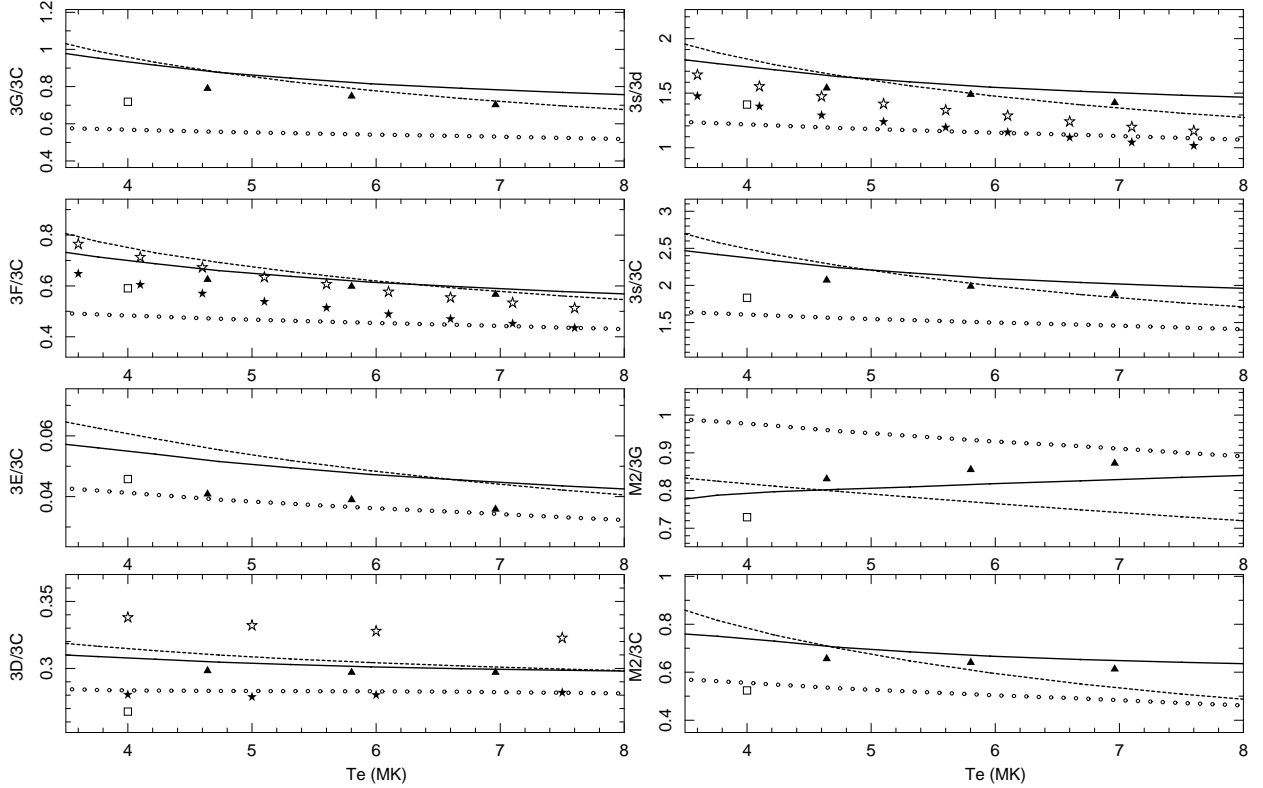


Fig. 1.— Comparison of Fe XVII line ratios in various theories. The solid line are those of Gu (2003); broken lines are those of Loch et al. (2006), open circles are from APEC, filled triangles are those of Doron & Behar (2002), open squares are from Bhatia & Doschek (2003), filled stars are those of Chen et al. (2003) for 3D/3C and 3F/3C ratio, and Chen & Pradhan (2005) for 3s/3d ratio, the open stars are those of Chen (2007) for the 3D/3C ratio. For 3F/3C and 3s/3d, the open stars are those of Chen et al. (2003) and Chen & Pradhan (2005) scaled for the updated 3C and 3D cross sections of Chen (2007).

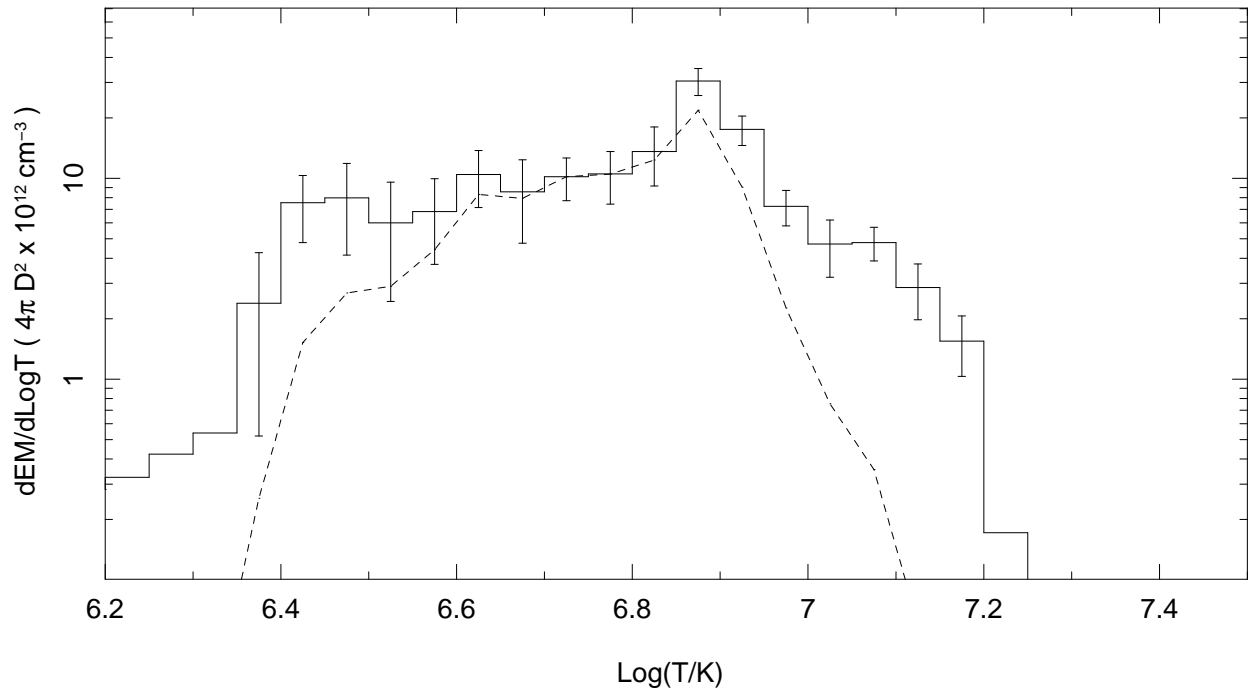


Fig. 2.— Reconstructed DEM of the combined Capella observation. D in the unit is the distance of the source in cm. The broken line show the total Fe XVII emissivity weighted DEM.

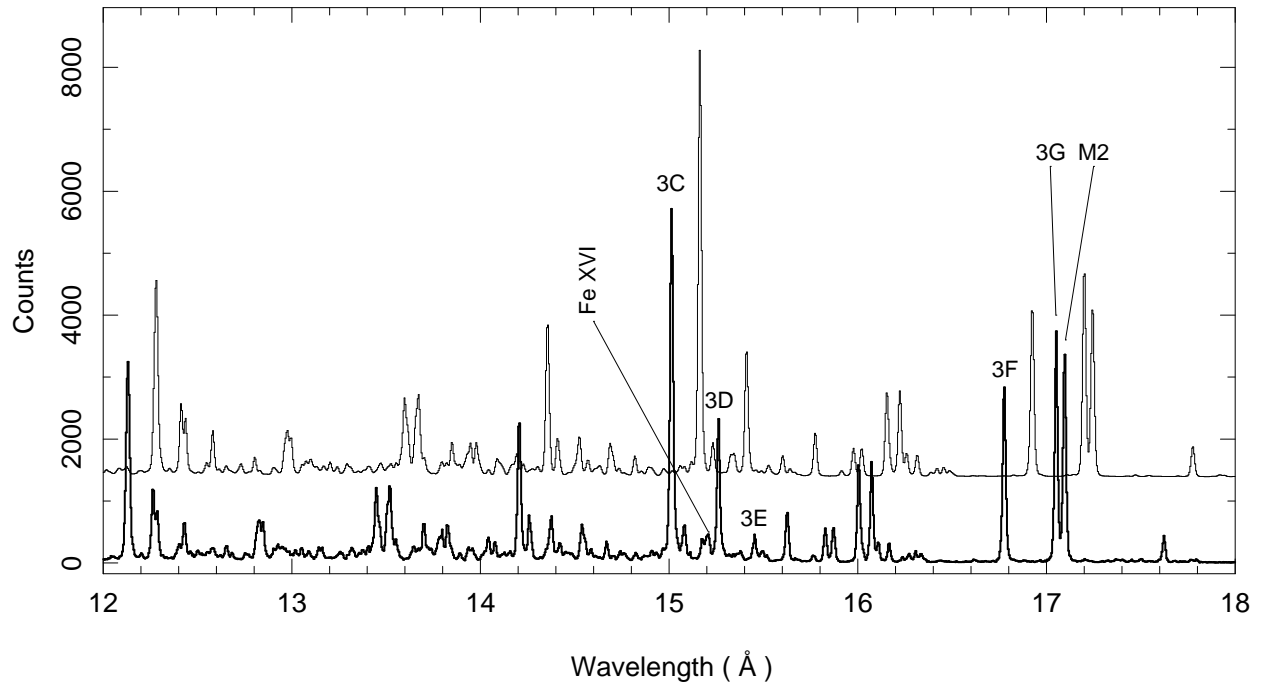


Fig. 3.— *Chandra* HETG spectrum of the combined observation of Capella in the 12–18 Å. The lower curve is the sum of ± 1 orders of MEG data, the upper curve is the model fit with the reconstructed DEM and elemental abundances, which is shifted to the upper-right for clarity. The Fe XVII lines and the Fe XVI line at 15.21 Å are marked.

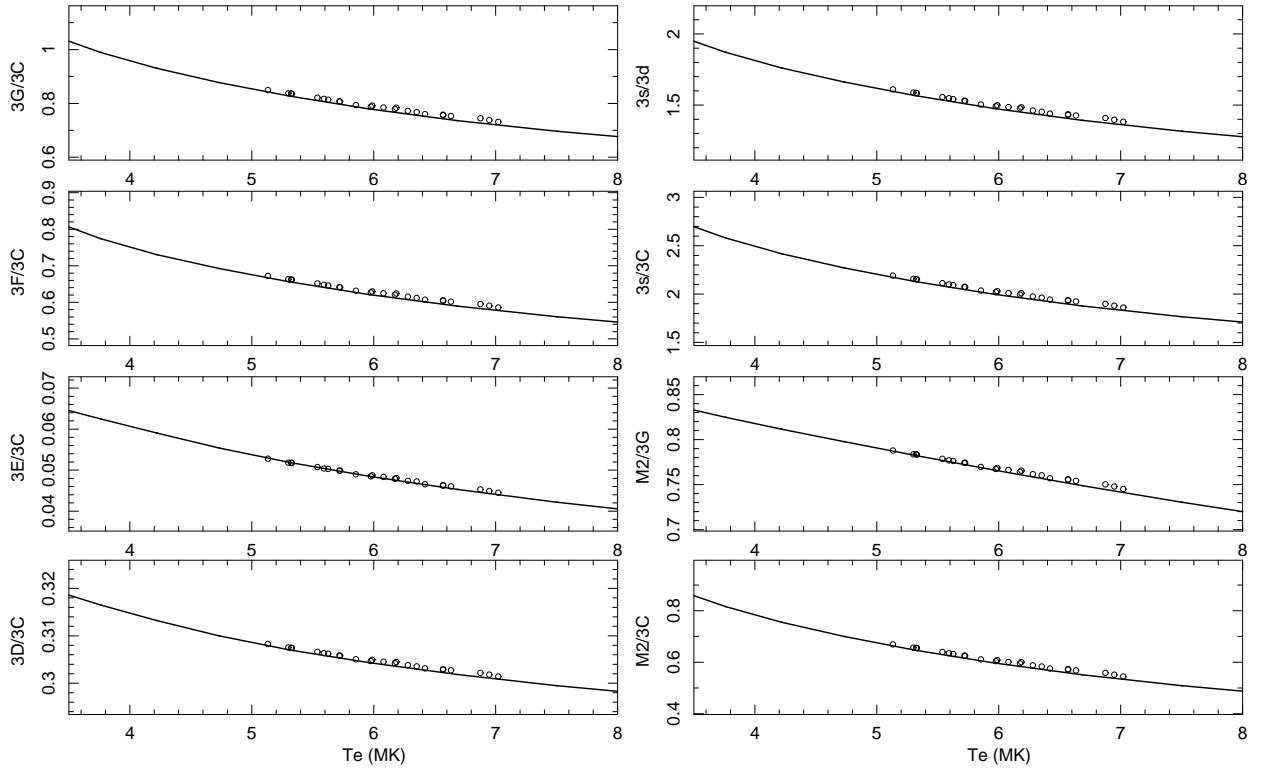


Fig. 4.— Comparison of Fe XVII line ratios calculated with the reconstructed DEM of the observations (solid lines), and those calculated at a single temperature of T_{em} (open circles).

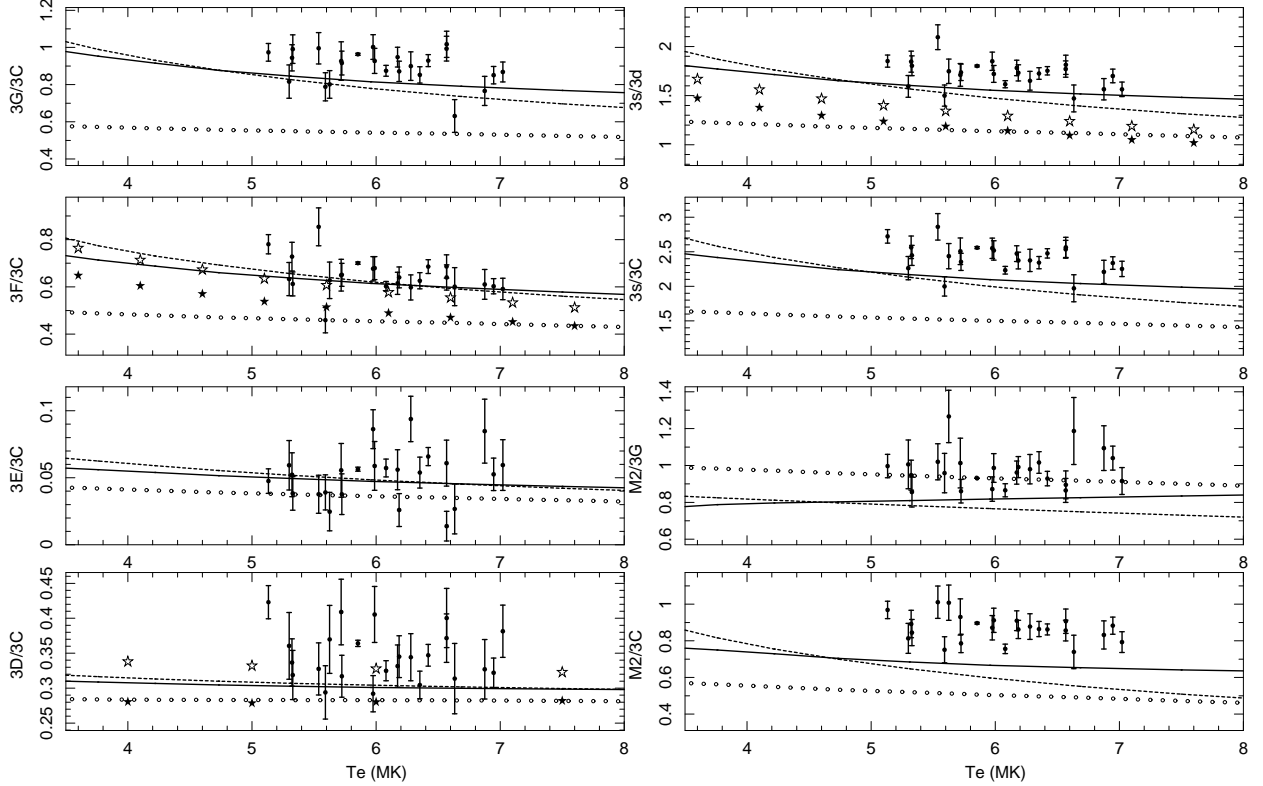


Fig. 5.— Comparison of measured and predicted Fe XVII line ratios. Filled circles with error bars are the measured values, solid lines are those of Gu (2003), broken lines are those of Loch et al. (2006), open circles are from APEC, , filled stars are those of Chen et al. (2003) for 3D/3C and 3F/3C ratio, and Chen & Pradhan (2005) for $3s/3d$ ratio, the open stars are those of Chen (2007) for the 3D/3C ratio. For 3F/3C and $3s/3d$, the open stars are those of Chen et al. (2003) and Chen & Pradhan (2005) scaled for the updated 3C and 3D cross sections of Chen (2007).

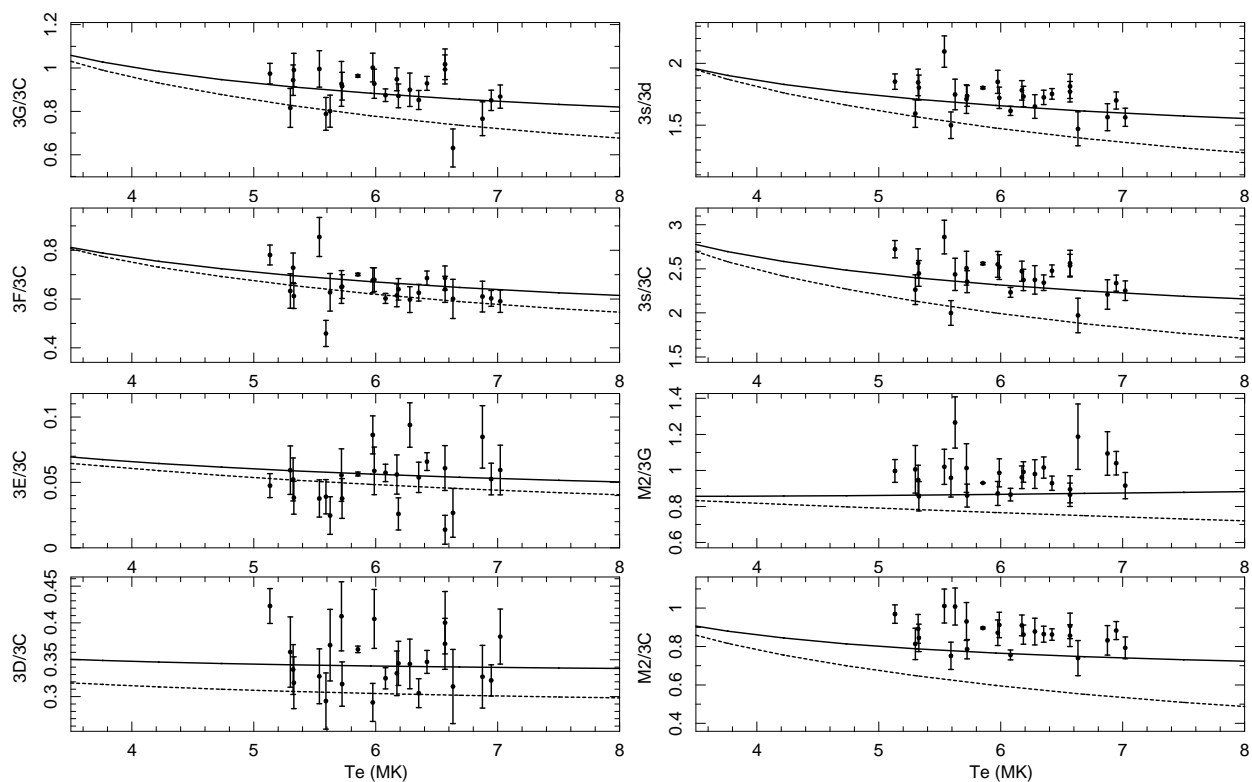


Fig. 6.— Comparison of measured Fe XVII line ratios with the predictions of the present MBPT corrected theory (solid lines). The predictions of Loch et al. (2006) are also shown as broken curves.

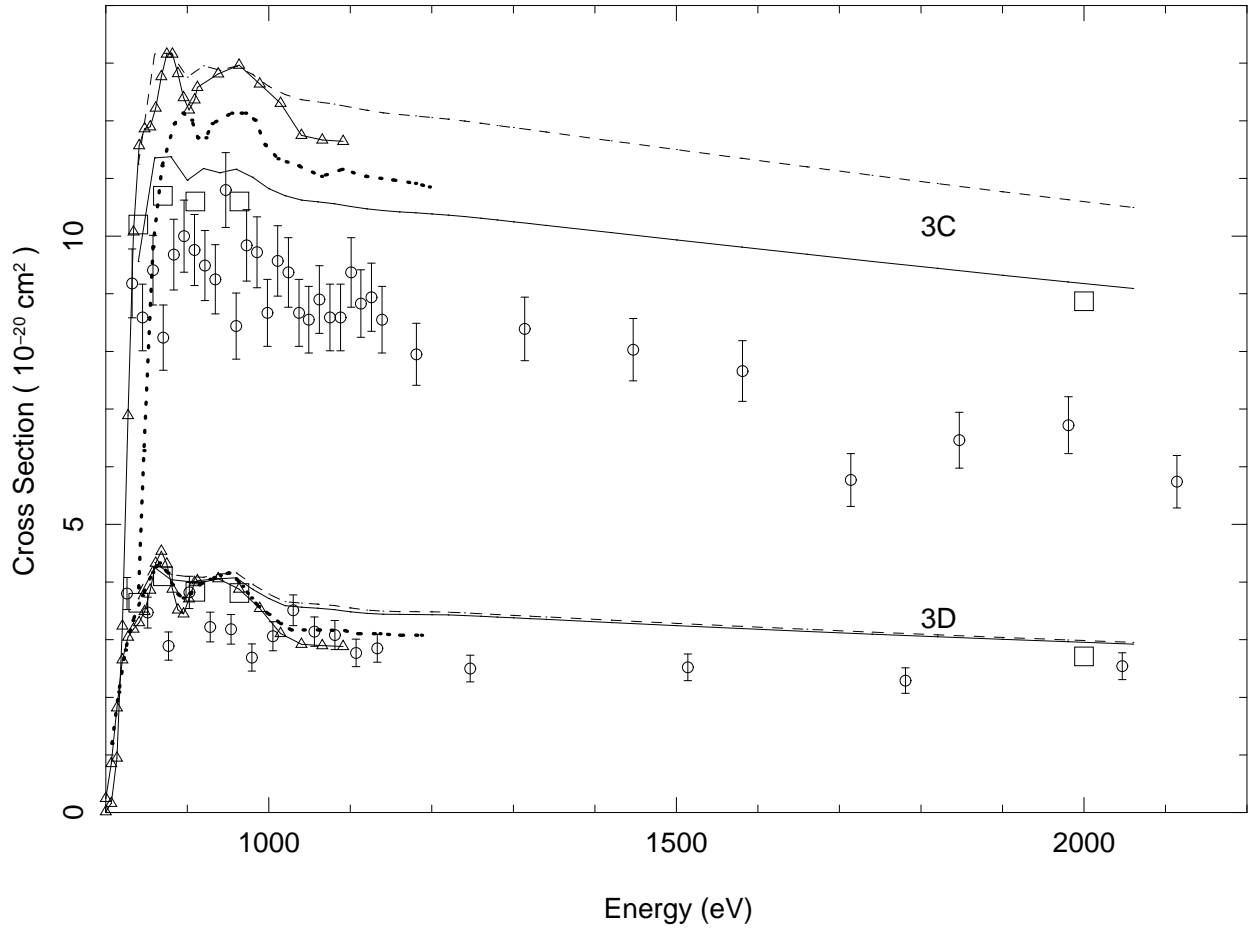


Fig. 7.— Comparison of measured and predicted 3C and 3D cross sections. The open circles with error bars are the laboratory measurements of Brown et al. (2006), solid lines with no symbols are the present MBPT corrected calculation, dashed lines are the values from Gu (2003), dotted lines are those of Loch et al. (2006), solid lines with filled triangles are those of Chen et al. (2003), and open squares are the calculations of Chen (2007).

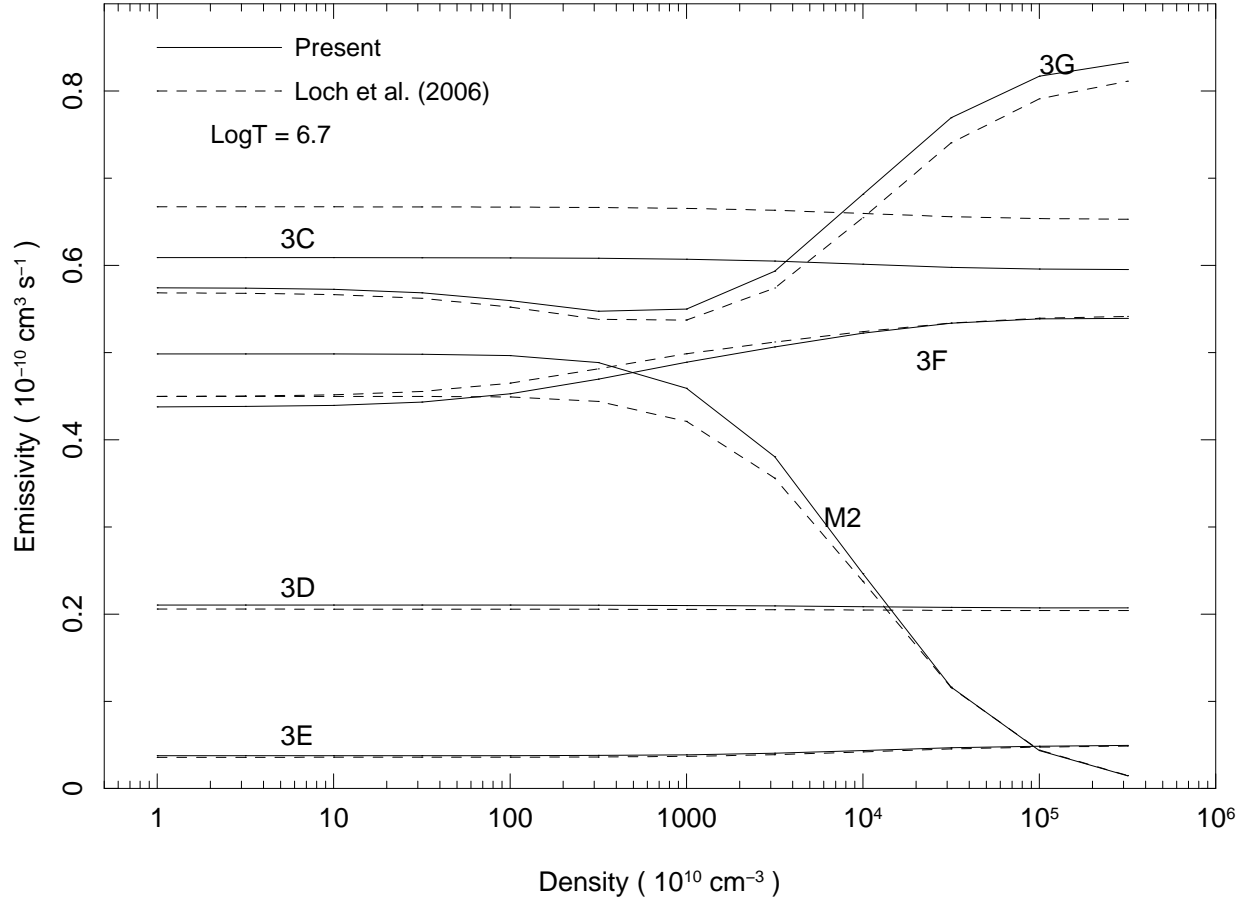


Fig. 8.— Density dependence of the Fe XVII line emissivity at a temperature of $10^{6.7}$ K. The solid lines are the present MBPT corrected calculations, and dashed lines are those of Loch et al. (2006).

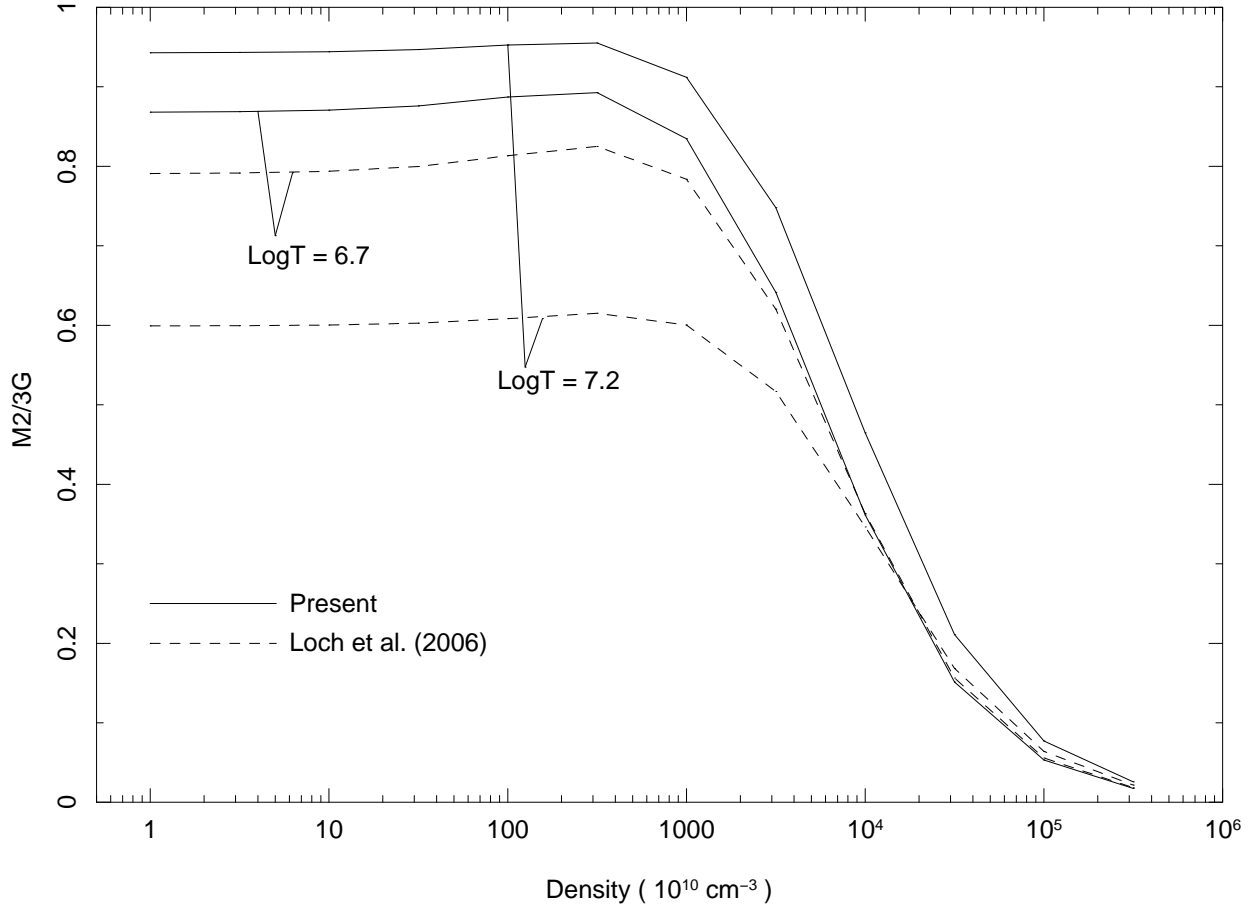


Fig. 9.— Density dependence of the M2/3G line ratio at two marked electron temperatures. The solid lines are the present MBPT corrected calculations, and dashed lines are those of Loch et al. (2006).